Research Square

Preprints are preliminary reports that have not undergone peer review.
They should not be considered conclusive, used to inform clinical practice,
or referenced by the media as validated information.

Metrology-Oriented Source-Point Sampling for Feature Continuity in Industrial Laser-Scanned Point Clouds

zhangchenlong huang

230248694@seu.edu.cn

Southeast University https://orcid.org/0009-0009-4629-6410

Haiying Wen

Zhijie Xia

Southeast University

Jia Fang

Southeast University

Yilin Tao

University of the West of England - City Campus: University of the West of England

Yibo Zhang

Southeast University

Zhisheng zhang

Southeast University

Research Article

Keywords:

Posted Date: November 13th, 2026

DOI: https://doi.org/10.21203/rs.3.rs-10574997/v1

License: This work is licensed under a Creative Commons Attribution 4.0 International License.
Read Full License

Metrology-Oriented Source-Point Sampling for Feature Continuity in Industrial Laser-Scanned Point Clouds

Zhangchenlong Huang [a], Haiying Wen*[a d],Zhijie Xia [a b], Fang Jia [a b],Yilin Tao [c], Yibo Zhang [a],Zhisheng Zhang*[a]

[a] School of Mechanical Engineering, Southeast University, Nanjing 211189, PR China

[b] National Innovation Center for Integrated Circuit Design Automation, No. 6, Changjiang Back Street, Xuanwu District, Nanjing City, 211189, PR China

[c] Bristol Robotics Laboratory,University of the West of England ,T Block Frenchay Campus, Coldharbour Ln, Bristol BS16 1QY

[d] State Key Laboratory of Mechanical Transmission for Advanced Equipment, Chongqing University, No. 174, Shazheng Street, Shapingba District, Chongqing City China

1. Abstract

Industrial laser scans are frequently reduced before geometric inspection, registration, and pose estimation. Such reduction can preserve broad surface coverage while interrupting the source-point sequences that support the estimation of hole rims, slots, interface edges, and related functional features. This paper presents a metrology-oriented source-point sampling method for industrial laser-scanned point clouds. The method assigns retention priorities to acquired points through a topology-guided protection field that combines local feature evidence, propagation along connected boundary segments, association across separated fragments, and attenuation outside feature regions. The selected cloud therefore remains a subset of the measured coordinates, rather than a set of generated replacements. The method was evaluated on ABC-derived workpieces, a controlled standard gauge, and high-voltage battery connector scans using reconstruction-oriented error, feature retention, edge-continuity dispersion, ablation tests, transfer without target fine-tuning, and a pose-oriented connector case study. At a 25% sampling rate, connector scans achieved 99.6% normalized feature recall and an edge-continuity dispersion of 0.0008. The pose case study reported a mean angular error of 3.77 degrees for three evaluated connector features. The results show that continuity-aware source-point selection can retain measurement-relevant boundary evidence under data reduction for the evaluated industrial scans.

Keywords: laser scanning metrology; source-point sampling; point-cloud down-

* *Corresponding Haiying Wen email： wenhy@seu.edu.cn*

* *Corresponding Zhisheng Zhang email： oldbc@seu.edu.cn*

sampling; traceability; feature continuity; edge-continuity error; industrial measurement

2. Introduction

In laser scanning metrology, down-sampling is not a neutral compression step because it can change the observations from which measurement features are estimated. Dense scans acquired for reverse engineering, digital metrology, and assembly inspection are often reduced before reconstruction, registration, boundary fitting, or pose evaluation (Blais, 2004; Salvi et al., 2010; Besl and McKay, 1992; Wang et al., 2020; Guo et al., 2020). The remaining problem is therefore not only computational efficiency. If source points on hole rims, edge loops, connector slots, or interface boundaries are removed or fragmented, the reduced cloud may remain visually plausible while the measurand-defining evidence becomes weaker. Thus, the central question of this paper is whether a reduced source-point set can preserve traceable and continuous measurement features under industrial scan conditions.

Coverage-oriented sampling provides the most direct answer to the data-volume problem. Voxel-grid filtering reduces redundancy by spatial quantization, random sampling offers a simple baseline, and farthest point sampling improves spatial spread by iteratively selecting points far from the current subset (Rusu and Cousins, 2011; Eldar et al., 1997). These methods solve the distribution side of down-sampling: they make the retained points more compact or more evenly dispersed. However, industrial measurement failures are often caused by local discontinuities rather than by global coverage alone. A sampling rule that treats all regions primarily through density or Euclidean distance may keep a visually well-spaced subset while breaking a narrow slot edge, a fractured hole contour, or an assembly interface.1

Feature-preserving simplification methods address this limitation by replacing uniform coverage with geometric salience. Early point-sampled surface simplification and point-set surface modeling showed that local surface variation, approximation error, and neighborhood structure can guide more meaningful reduction (Pauly et al., 2002; Alexa et al., 2003). Later graph and feature-preserving formulations further combine local geometry, graph resampling, curvature, normal variation, and uniformity control to protect salient regions during simplification (Chen et al., 2018; Qi et al., 2019; Xu et al., 2022). These studies answer an important question: which points look geometrically important in a local neighborhood. They do not fully answer a metrology-specific question: how to keep several locally separated fragments as one continuous measurement feature when the scan contains occlusion, density asymmetry, chipped edges, or discontinuous hole boundaries.234[56]

Learning-based sampling then moves the field from hand-designed criteria to

trainable point selection. S-NET learns a representative reduced set, Gumbel subset sampling and SampleNet make point selection differentiable, and task-oriented or learnable feature-preserving samplers optimize reduction under downstream or reconstruction-driven objectives (Dovrat et al., 2019; Yang et al., 2019; Lang et al., 2020; Qian et al., 2020; Potamias et al., 2022). These works solve the problem of adaptation: the sampler can be optimized for representation, reconstruction, or task performance instead of relying only on fixed geometric rules. Yet they do not by themselves define an industrial source-point continuity constraint. Generated or relaxed sampling points may need projection back to the input, while reconstruction or classification losses can still under-penalize a broken edge loop if the global shape remains plausible.78[910]

A related stream studies domain adaptation and generalization for 3D point clouds. PointDAN, geometry-aware self-training, and single-sample generalization methods reduce the domain gap for point-cloud representation, mainly in classification or segmentation settings (Qin et al., 2019; Zou et al., 2021; Wei et al., 2022). This line is useful because industrial scans differ from academic datasets in scale, density, noise, and feature composition. However, transferring a semantic representation is not equivalent to transferring a sampling decision for source points. A classifier can tolerate redistributed features as long as the category remains recognizable; a measurement pipeline cannot, because a broken boundary or displaced source point can change the pose, radius, or interface estimate even when the global object shape appears acceptable.111213

The measurement-science gap addressed in this paper is therefore more specific than general point-cloud compression or generic learning-based sampling. Industrial laser-scan down-sampling needs a representation in which traceable source points and feature continuity are treated as measurement-data properties. The object to be preserved is not merely an isolated high-curvature point, nor only a low Chamfer Distance reconstruction, but a source-point structure that remains connected along boundaries used for geometric estimation. This perspective explains why local feature scores, global uniformity, and reconstruction-driven losses can all be insufficient: each captures part of the geometry, but none directly represents continuity loss in fragmented yet functionally connected measurement features.

To address this gap, this paper develops a topology-guided source-point sampling framework for industrial laser-scanned data. The central idea is to encode feature continuity as a protection field on a multi-scale source-point graph. Local geometric evidence initializes feature activation; local propagation maintains continuity along edges and corners; non-local association links structurally related fragments; and a feedback attenuation term suppresses uncontrolled diffusion into flat regions. This design keeps the selected subset tied to acquired coordinates while reallocating the sampling budget

toward measurement-critical structures. The study evaluates this formulation on a controlled standard gauge and industrial battery-connector scans, using feature retention, edge-continuity dispersion, cross-domain transfer, and pose-oriented validation to examine whether the representation supports measurement tasks.

The main contributions are threefold. First, this paper formulates industrial point-cloud down-sampling as a metrology-oriented source-point reduction problem, rather than as a purely uniform coverage or reconstruction problem. This formulation makes the measurement object explicit: preserving traceable source points and the connected structure of functional boundaries under data reduction.

Second, STDN introduces a topology-guided protection representation for source-point selection. By combining local propagation, non-local feature association, and feedback-controlled attenuation, the method is designed to protect continuous and fractured feature lines while avoiding unlimited expansion of high weights into flat regions. The innovation lies in using topology to organize which acquired points should be protected, not in simply stacking a larger network around a conventional sampler.

Third, the paper builds an industrial validation setting that connects sampling quality with measurement consequences. The experiments include standard-gauge and battery-connector scans, report feature recall and edge-continuity dispersion in addition to reconstruction-oriented metrics, and examine whether boundary-preserving sampling supports pose-related inspection on connector features. These results provide a focused basis for assessing traceable source-point sampling in industrial laser scanning metrology.

2. Related Work

2.1 Point Cloud Simplification and Filtering Methods: Uniform-Coverage-Based Strategies

Coverage-based simplification methods such as FPS reduce sampling randomness by distributing points over the object surface, but this objective can overlook sparse functional boundaries. Figure 1 illustrates how coverage-driven selection can fragment narrow edge regions.[14][15]

Let the original point cloud and the current sampled set be denoted by the variables in Eq. (1). FPS selects the next point by maximizing its minimum distance to the current sampled set:

$$p_{\text{next}} = \arg\max_{p \in P \setminus S} \left(\min_{s \in S} \| p - s \|_2 \right) \tag{1}$$

Figure 1 summarizes this limitation: a globally well-spaced subset may still miss points along a disconnected or narrow feature.[16][17]

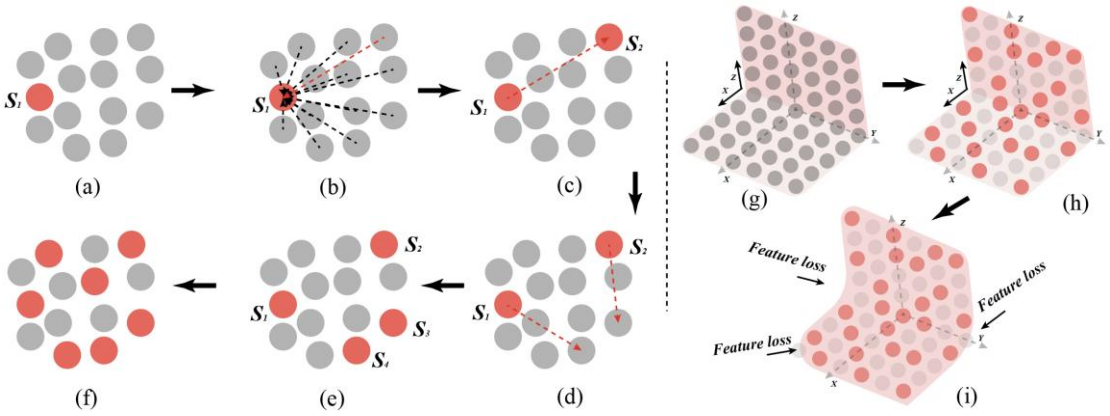


Figure 1: Uniform-coverage sampling and feature-fragmentation risk.

2.2 Feature-Preserving Strategies Based on Local Geometric Analysis

Local-geometry methods improve feature sensitivity by weighting curvature, normals, or neighborhood statistics, but their decisions remain largely pointwise.[18]

$$W(p) = \alpha \cdot w_d(p) + \beta \cdot w_e(p) + \gamma \cdot w_n(p) \quad (2)$$

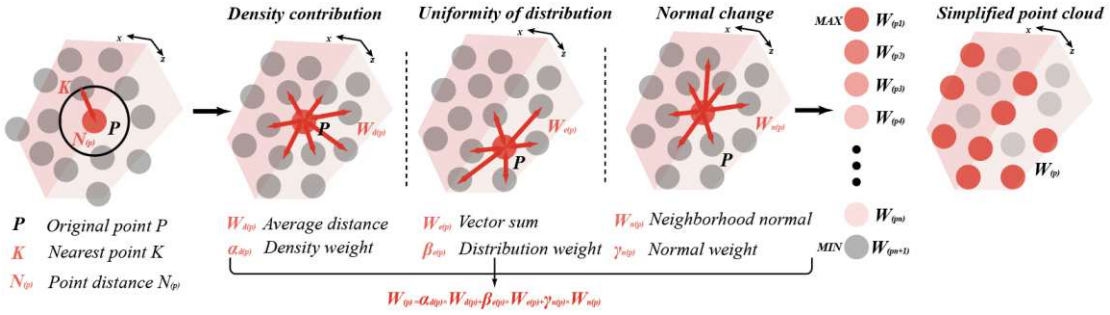


Figure 2: Local-geometry feature retention strategy.

This local weighting helps retain sharp points, yet it does not explicitly protect feature-line continuity or closed-loop structures.[19][20]

2.3 Learning Strategies Based on Metric Loss

Learning-based samplers such as SampleNet and S-NET optimize differentiable reconstruction or sampling losses. This improves task adaptation but does not, by itself, encode the continuity of functional boundaries.[21]

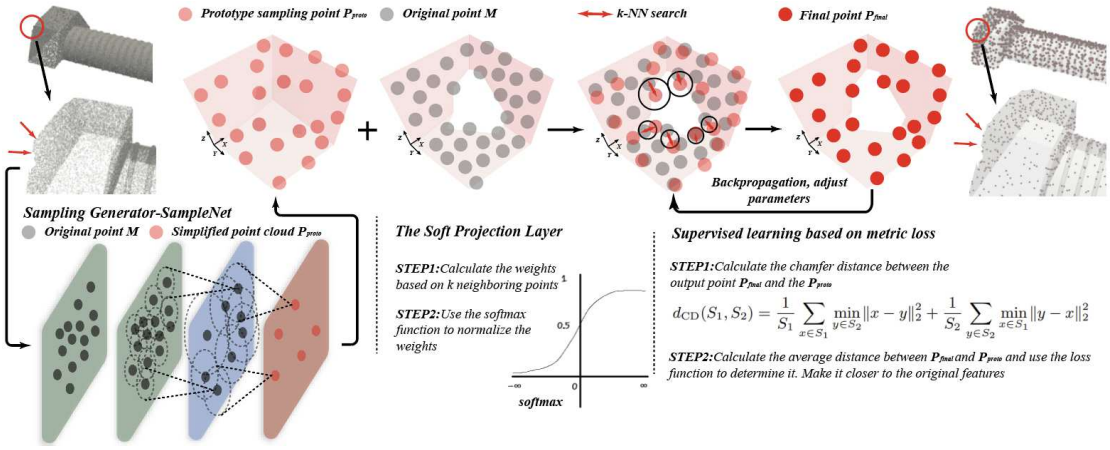


Figure 3: Metric-loss-driven learning strategy.

Chamfer Distance mainly measures spatial coverage and nearest-neighbor reconstruction error:

$$d_{CD}(P_{final},M)=\frac{1}{|P_{final}|}\sum_{x\in P_{final}}\min_{y\in M}\|x-y\|_2^2+\frac{1}{|M|}\sum_{y\in M}\min_{x\in P_{final}}\|y-x\|_2^2 \quad (3)$$

Consequently, CD-driven learning may preserve global coverage while under-penalizing local breaks in holes, corners, and edge loops.[2223]

2.4 Topology-aware propagation for measurement feature continuity

Collective behavior is used only as a computational analogy for stable neighborhood interaction, not as a biological claim. The relevant abstraction is a topology-aware propagation process in which local interactions preserve coherent structures.[24]

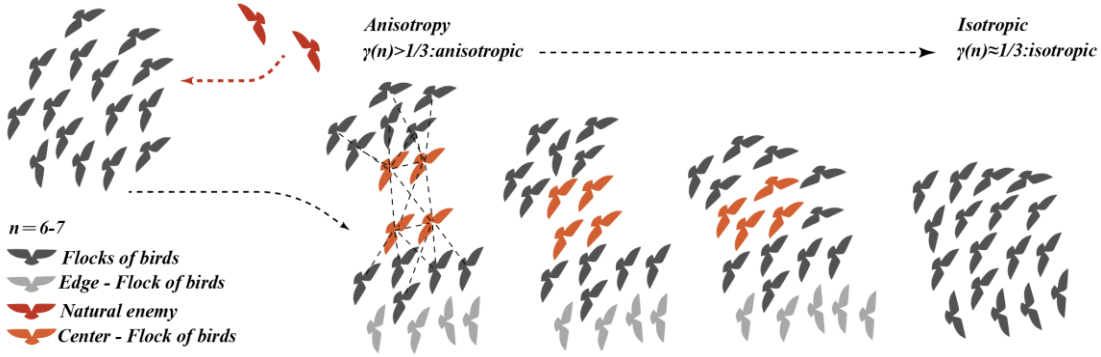


Figure 4: Topological interaction analogy for neighborhood influence.

In STDN, this abstraction is translated into point-wise protection weights and neighborhood contribution scores; its measurement role is to preserve functional boundary continuity during point-cloud reduction.

2.5 Continuity-preserving source-point sampling model

The remaining modeling problem is to propagate protection signals across both continuous and fractured features while suppressing diffusion into flat regions.[25]

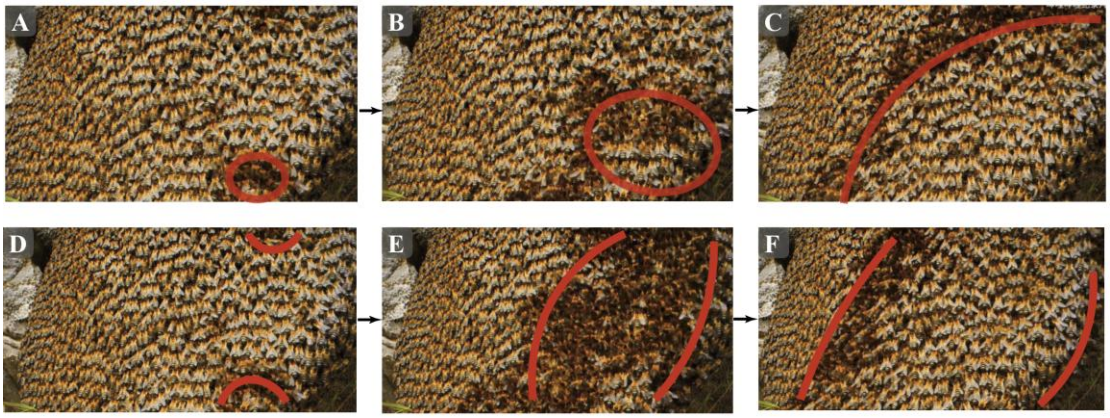


Figure 5: Propagation analogy for feature-protection signals.

STDN therefore combines local topological propagation for continuous edges with non-local association for fractured structures. The analogy serves only to motivate these computable mechanisms.[2627]

$$\lambda = \frac{P(\theta)/r^2 + \varepsilon}{1 + P(\theta)/r^2 + \varepsilon} \tag{4}$$

Here, the bias term prevents complete gradient disappearance in flat regions, while anisotropy controls whether a neighborhood can transmit feature protection.

The dynamics are abstracted into three node states: inactive redundant points, active feature points, and attenuated transition points.[28]

Table 1 summarizes the heuristic mapping between propagation roles and point-cloud graph components. This mapping provides the computational basis for the subsequent dynamic propagation module.

Table 1: Heuristic mapping from propagation analogy to STDN graph components.

Bees	A point in the point cloud	Identify the basic node units in the computational graph.
Wasp	Downsampling operation	Reduction operation on the cardinality of a set.
"Flashing" state	The protection weight/retention probability of the point	The attribute values obtained by the node to avoid being removed.
"Inactive" state	Ordinary level	Nodes with lower weights/probabilities, default state.
"Active" state	Key feature points.	Nodes with extremely high weights/probabilities act as the sources of propagation.

"Stasis" state	Transition area point	Nodes with temporarily reduced weights are used to suppress the propagation.
Producer	Extremely curved point	Initial activation source for the protection signal.
Bucket chain conveyor	Points with higher curvature nearby	Carry out local topological propagation of the protection signal along the continuous feature lines.
Tail of the chain	Transition point between features and flat areas	Receive the signal but no longer transmit it, achieving the termination of the protected signal in the flat area.
Transmission rate	Confidence level of feature transfer	The probability of weight transmission between nodes is related to the geometric anisotropy of the topological neighborhood.
Fatigue rate	Weight decay rate	The rate at which node weights transition from the active state to the dormant state.

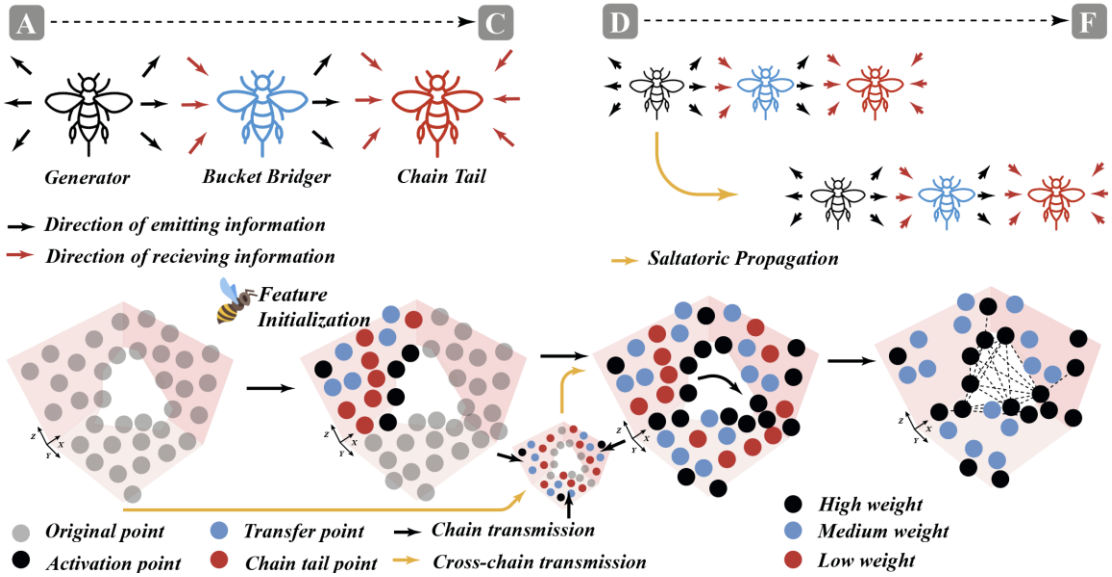


Figure 6: Local and non-local propagation prototypes.

These abstractions define two sampling operations: local propagation along continuous boundaries and non-local linking of fractured but structurally related features.

For continuous high-curvature edges, activation propagates through local graph neighbors so that adjacent boundary points receive compatible protection weights.

1. Feature initialization: points with high local curvature are selected as initial activation sources and assigned high protection weights.
2. Signal termination: when activation reaches the transition between feature and flat regions, propagation is attenuated to confine high weights to the feature line.

For fractured edges, non-local links connect structurally related but spatially separated points, reducing the risk that sampling breaks a functional loop.[29]

3. Topology-Guided Source-Point Sampling Methodology

STDN learns a source-point sampling function that assigns each input point a protection weight and selects a subset for downstream inspection.

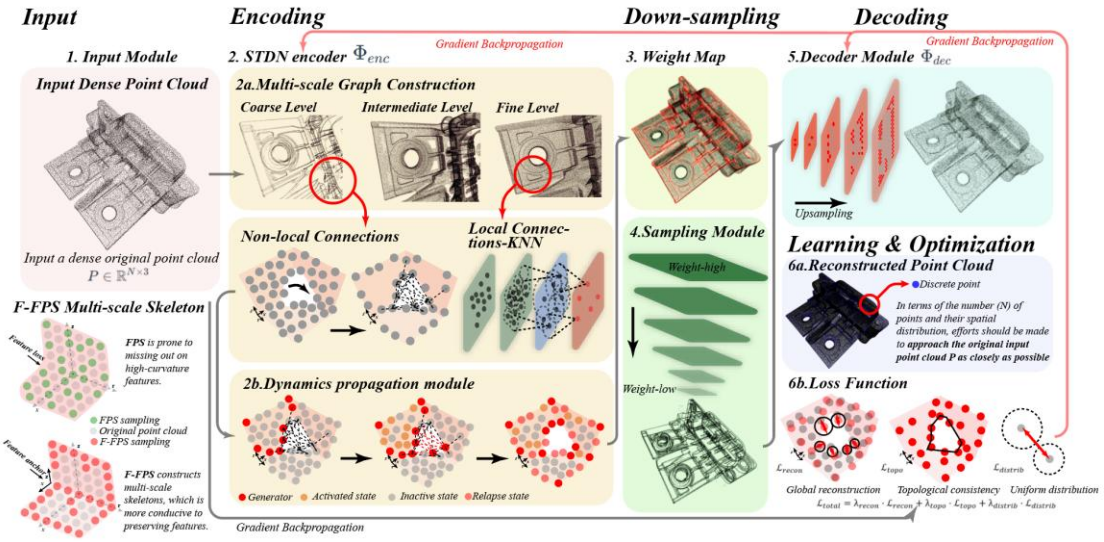


Figure 7: STDN framework for topology-guided source-point sampling.

Figure 7 gives the pipeline: the encoder builds topology-guided weights, Top-K selection keeps acquired source points, and the decoder provides self-supervised reconstruction feedback.

Minimizing the discrepancy between the reconstructed cloud and the original input jointly optimizes the encoder and decoder parameters.

3.1 Topology-Guided Protection Field for Measurement Features

The STDN encoder assigns a protection weight to each point on a multi-scale graph so that boundary continuity, rather than pointwise curvature alone, guides sampling.

2.1 Construction of the Multi-scale Topological Graph

To capture non-local structures without incurring full-graph complexity, STDN constructs a multi-scale surrogate graph. Because conventional FPS is insensitive to geometric curvature, a feature-weighted FPS strategy extracts skeleton nodes using a metric that combines Euclidean distance with local geometric features:[30]

$$D(p,s) = \alpha|p-s|_2^2 + (1-\alpha)|F_p - F_s|_2^2 \quad (5)$$

The variables in Eq. (5) denote local curvature, normal-eigenvector information, and a balancing hyperparameter between spatial coverage and feature salience. This feature-weighted metric preserves the global skeleton while anchoring high-frequency geometric structures.[31]

The multi-scale graph contains both local and non-local edges. Local edges are obtained by K-nearest-neighbor search on the full-resolution point cloud and provide short-range propagation paths for protection signals.

Non-local edges are defined on the sparse skeleton to bridge fractured features. Each original point is mapped to a representative skeleton point; if two skeleton points are neighbors on the skeleton K-NN graph, their corresponding original points are connected by a non-local edge:

$$\mathcal{E}_{non-local} = \{(i,j) \mid (M(p_i), M(p_j)) \text{ is an edge in } \mathcal{G}^{(L)}\} \tag{6}$$

This construction links structurally related points and allows fractured features to remain connected during sampling.[3233]

3.2 Adaptive Dynamics Propagation Module

On the constructed graph, STDN iteratively updates node states to generate the final protection-weight map.

The H-R module propagates feature activation on the hybrid graph while attenuating isolated noise responses.[3435]

$$\theta_i = \Psi_{params}(F_i) \tag{7}$$

At each time step, a node first aggregates stimuli from its multi-scale topological neighborhood:

$$I_{i,t} = \sum_{p_j \in \mathcal{N}(p_i)} \lambda_{ij} x_{j,t} \tag{8}$$

The learnable transmission rate represents confidence in neighborhood information transfer. The aggregated stimulus is then passed to the nonlinear dynamics core for joint feature enhancement and noise suppression:

$$\begin{cases} x_{i,t+1} = x_{i,t} + h\left(y_{i,t} - a_i x_{i,t}^3 + b_i x_{i,t}^2 - z_{i,t} + I_{i,t}\right) \\ y_{i,t+1} = y_{i,t} + h\left(c_i - d_i x_{i,t}^2 - y_{i,t}\right) \\ z_{i,t+1} = z_{i,t} + h[r_i(s(x_{i,t} - x_{rest}) - z_{i,t})] \end{cases} \tag{9}$$

The fatigue variable regulates stability and feature selectivity through negative feedback. Continuous edges sustain activation through neighborhood support, whereas isolated high-frequency responses decay because they lack topological reinforcement. This state-memory mechanism distinguishes the propagation module from standard graph message passing and motivates the ablation tests reported later.[36]

After the fixed propagation depth, the Sigmoid-normalized activation value is used as the final protection weight for Top-K source-point selection.

4. Self-supervised Loss Function

The self-supervised objective combines global reconstruction, local topological consistency, and spatial regularization.

$$\{\mathcal{L}_{total} = \lambda_{recon} \cdot \mathcal{L}_{recon} + \lambda_{topo} \cdot \mathcal{L}_{topo} + \lambda_{distrib} \cdot \mathcal{L}_{distrib} \quad (10)$$

In Eq. (10), the three loss terms correspond to global geometric reconstruction, topological consistency, and spatial distribution regularization; the hyperparameters balance their relative contributions.

The Chamfer reconstruction term keeps the sampled set informative for global shape recovery.[37]

$$\mathcal{L}_{recon}(P, P_{\text{recon}}) = \frac{1}{|P|}\sum_{p\in P} \min_{p'\in P_{recon}} \| p - p' \|_2^2 + \frac{1}{|P_{recon}|}\sum_{p'\in P_{recon}} \min_{p\in P} \| p' - p \|_2^2 \quad (11)$$

This term contains completeness and accuracy components, which respectively encourage coverage of the original model and geometric fidelity of the reconstructed result.

The topological consistency term addresses CD's weak sensitivity to local continuity by smoothing protection weights within graph neighborhoods.[38]

For each point and its K-nearest neighbors in the local graph, the topological consistency term penalizes deviations between the point protection weight and the neighborhood average. Weighting this penalty by the point's own protection weight focuses the regularization on critical feature regions:

$$\mathcal{L}_{topo} = \frac{1}{N}\sum_{p_i\in P} w_i \cdot \frac{1}{K}\sum_{p_j\in N(p_i)} (w_i - w_j)^2 \quad (12)$$

This penalty encourages neighboring points on the topological graph to receive compatible protection weights, helping feature signals propagate along continuous structures.

To prevent feature weights from diffusing into geometrically flat regions, the H-R fatigue variable acts as a negative-feedback term. The resulting objective balances local continuity against sparsification, allowing feature protection to remain localized.

The uniformity regularizer prevents collapse of the selected subset and maintains global object coverage.[39]

$$\mathcal{L}_{distrib} = \sum_{s_i\in P_{sub}} \sum_{s_j\in P_{sub}, j\neq i} max(0, r_d - \| s_i - s_j \|_2)^2 \quad (13)$$

Together, these terms restrict the solution space to subsets that retain both global coverage and task-relevant boundary continuity.

The final parameters are learned by gradient descent under this composite objective.

4. Experiments and Validation

The experiments evaluate feature preservation, module contribution, transfer across tested scan domains, industrial geometric fidelity, and downstream pose error.

4.1 Controlled Standard Gauge Data Acquisition

Two scan categories are used: a controlled standard-gauge benchmark and complex battery-connector components, both acquired with the same high-precision laser scanning system.

Dataset A is a precision trapezoidal gauge with controlled WEDM defects, providing reference edges, planes, and holes for feature-retention evaluation.

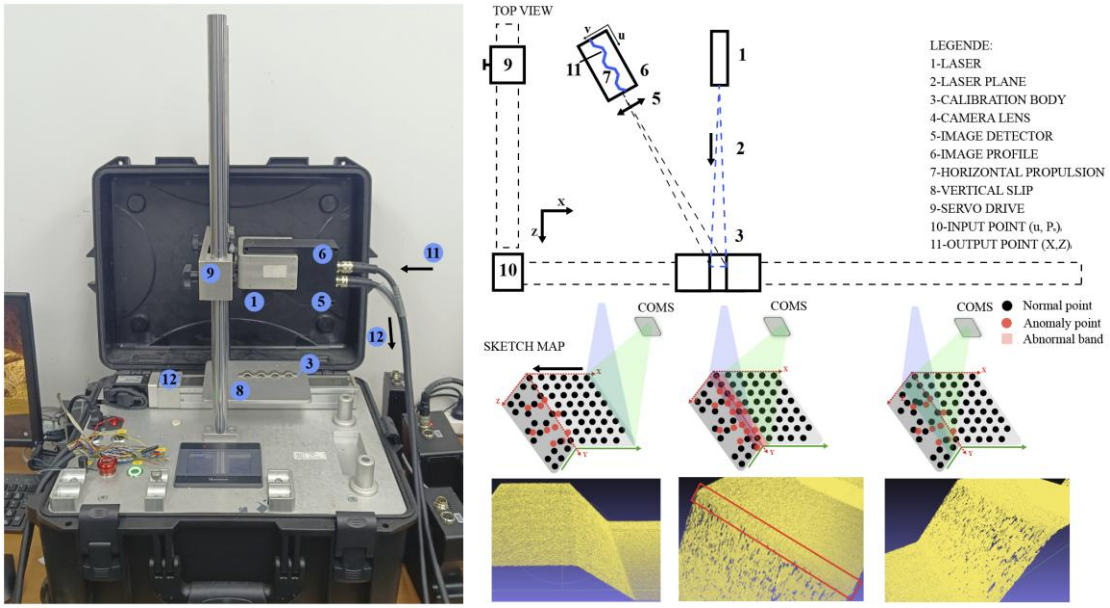


Figure 8: Data acquisition and data quality.

Single-path scanning introduces direction-dependent fidelity differences, making the gauge suitable for testing feature preservation under realistic acquisition bias.

4.2 Acquisition of New Energy High-Voltage Female Connector Sockets

Dataset B consists of feature-dense battery connectors with fractured holes, assembly interfaces, and discontinuous boundaries.

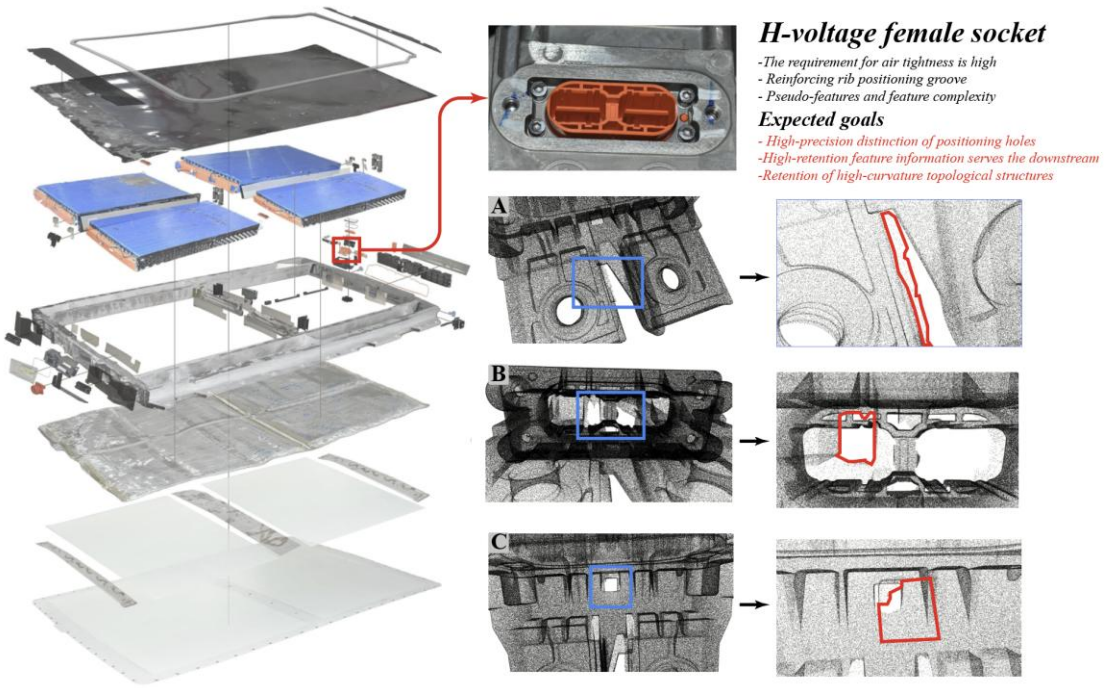


Figure 9: High-voltage battery pack dataset acquisition and data quality.

Figure 9 illustrates chipped holes, fractured edges, and local discontinuities in the connector scans, which are the structures targeted by topology-guided sampling.

4.3 STDN Training Data Flow and Quantitative Configuration

Models are trained on ABC-derived data and tested, without fine-tuning, on the standard-gauge and connector scans; all methods use the same preprocessing and sampling ratio.

Table 2 summarizes the implementation settings, including Adam optimization, learning-rate decay, loss weights, and propagation depth.

Table 2: Configuration of Regular Terms and Their Corresponding Relationships

Weight name	Numerical value	Objective
Weighted discrimination constraint λ_{recon}	0.5	Encourage protection weights to stratify point importance.
Topological consistency constraint λ_{topo}	0.005	Stabilizing the propagation of H-R dynamic signals on the topological connection
Uniformity of distribution constraint $\lambda_{distrib}$	0.05	The spatial coverage used to constrain the weight graph W

The selected configuration balances convergence speed and continuity of the learned protection weights.

4.4 Training Convergence and Hyperparameters

Figure 10 indicates that protection weights stabilize after early training, supporting the selected training length and hyperparameter setting.

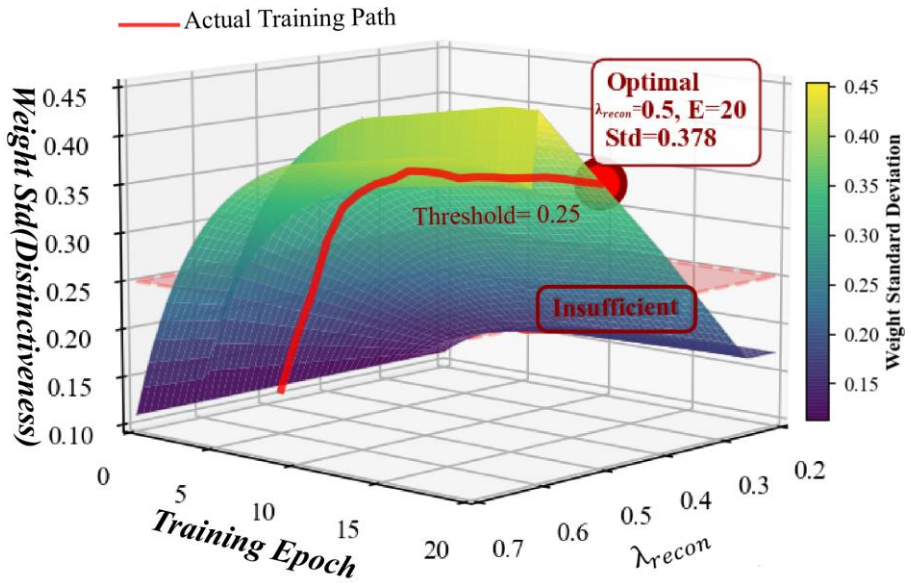


Figure 10: STDN training convergence and hyperparameter behavior.

4.5 Validation of H-R Dynamics

The ablation study uses a bearing sleeve from the ABC dataset with annotated edge and corner points to test whether the dynamic and topological components contribute to feature retention.

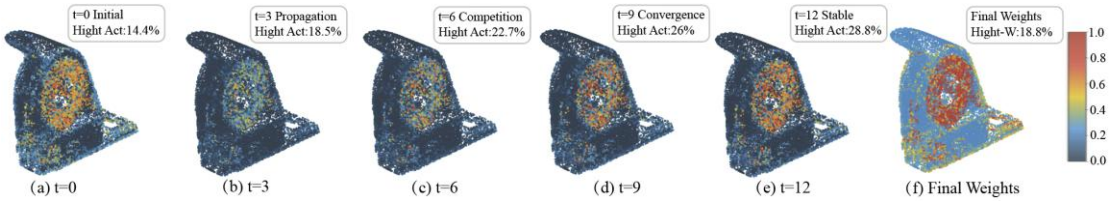


Figure 11: Time-series evolution of H-R dynamics.

Figure 11 visualizes activation spreading from sparse high-response points to continuous boundary regions during propagation.

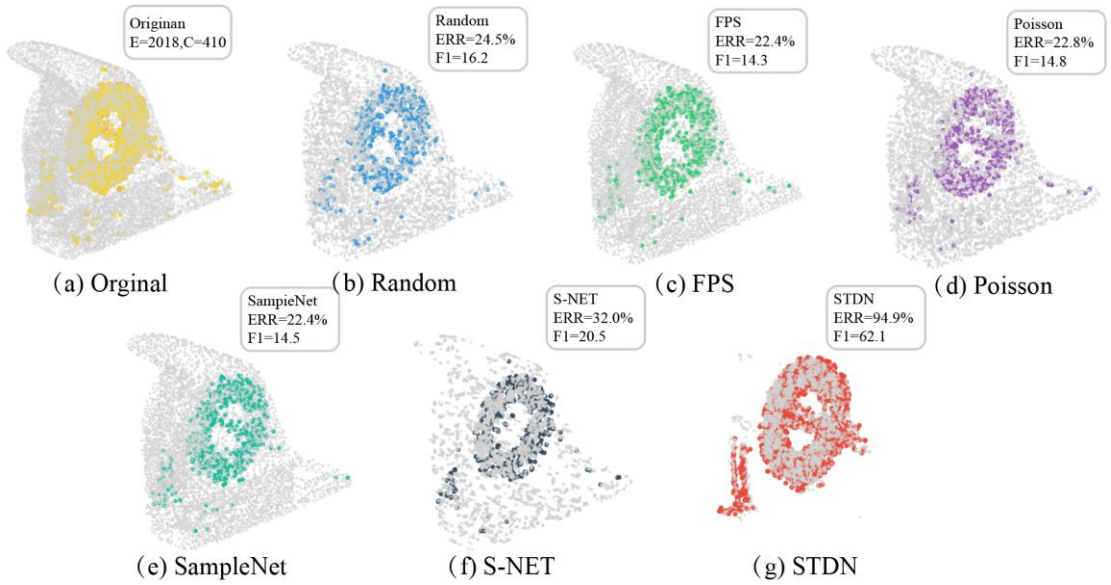


Figure 12: Feature preservation comparison among six samplers.

Table 3: Comparison of Feature Preservation Performance of Six Sampling Methods

Method	Edge point (E)	Corner (C)	ERR%	CRR%	F1
Random	502	110	24.5	26.8	16.2
FPS	459	83	22.4	20.2	14.3
Poisson Disk	467	93	22.8	22.7	14.8
SampleNet	459	91	22.4	22.2	14.5
S-NET	656	120	32.0	29.3	20.5
STDN	1915	408	94.9	99.5	62.1

Table 3 reports that STDN achieves 94.9% ERR, 99.5% CRR, and 62.1 F1 on the tested workpiece, indicating higher feature retention than the selected baselines in this setting.

4.6 Ablation Study of Sampling Strategies

Four ablations isolate the effects of H-R dynamics, topology construction, and adaptive propagation.

Table 4: Results of STDN Sampling Strategy Abandonment Experiment

Configuration	ERR(%)	CRR(%)	ΔERR
Complete STDN	94.9	99.5	/
w/o H-R	1.8	0.5	-98.1%
w/o Topology	24.0	23.4	-74.7%
w/o Adaptive	24.4	24.6	-74.3%

Removing H-R dynamics or topology sharply reduces ERR and fragments the sampled distribution, indicating that both propagation and graph structure contribute under this evaluation.

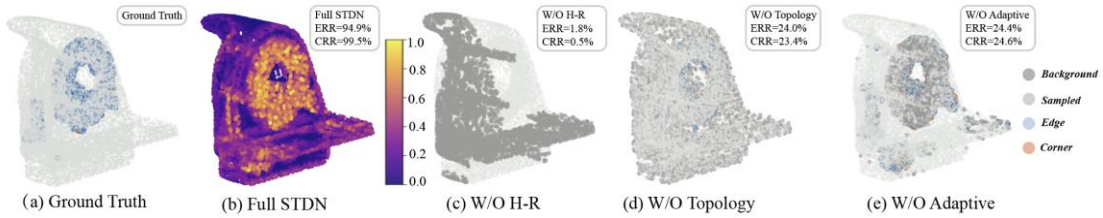


Figure 13: Visual ablation of STDN sampling strategies.

Figure 13 qualitatively supports Table 4: full STDN concentrates weights along edges, whereas ablated variants produce sparse or fragmented responses.

4.7 Effectiveness of Topological Constraints

Topological consistency is further evaluated on connector holes using Neighborhood Weight Variance (NWV), where lower values indicate smoother feature-region weights.

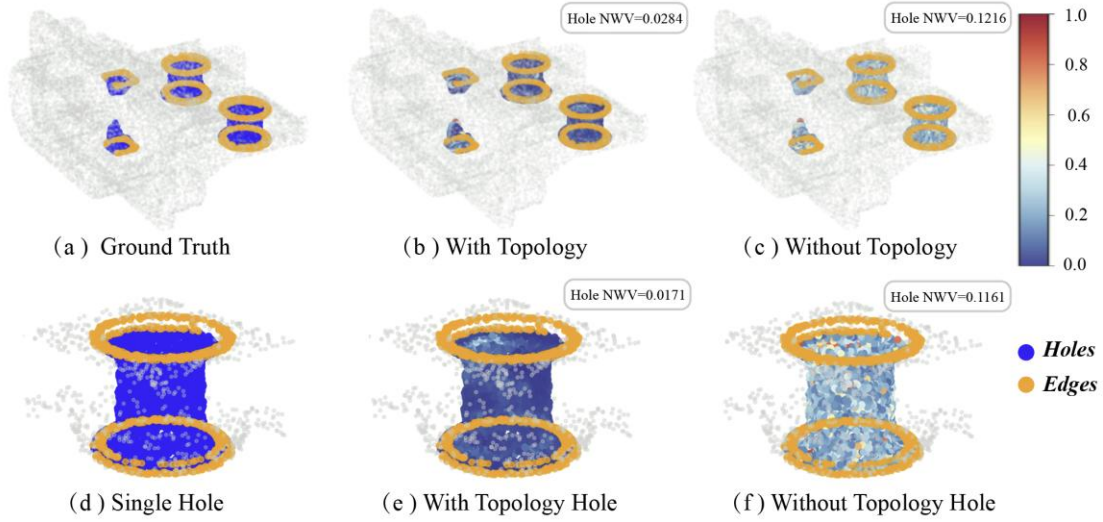


Figure 14: Effect of topological constraints on weight continuity.

Table 5: The Impact of Topological Constraints on the Smoothness of Sampling Weights at Different Spatial Scales

Region	Points	STDN NWV	w/o Topology NWV	Absolute difference Δ
Global	7106	0.088	0.160	+0.072
Hole area	5510	0.028	0.122	+0.094
Single hole	~920	0.017	0.116	+0.099

Table 5 reports that removing topology increases NWV across scales, indicating less coherent protection of hole regions.

Figure 14 visualizes this effect: topology-enabled weights are more uniform around holes, whereas the ablated model gives mottled feature responses.

4.8 cross-domain transfer Validation

The transfer test evaluates whether ABC-trained models retain performance on industrial scans without target-domain fine-tuning.

The three domains differ in geometric complexity: ABC, the standard gauge, and the battery connector.

Table 6 summarizes domain complexity using curvature variation, high-curvature ratio, and a composite topological score.

Table 6: Geometric complexity metrics quantifying domain discrepancies.

Data set	CV	HCR	TS	Overall score	Complexity level
Standard Rail	0.611	0.100	0.044	28.78	Complexity level
ABC	0.758	0.151	0.151	39.38	Medium
Battery Pack	1.228	0.100	0.084	54.65	Complex

Table 6 confirms that the connector is the more complex industrial domain, with higher curvature variation and topological complexity than the gauge.

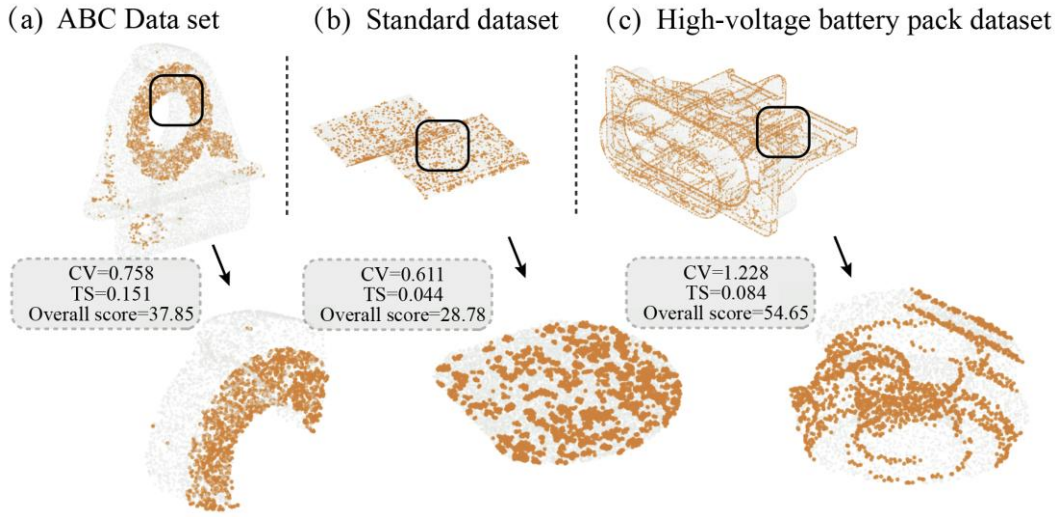


Figure 15: Dataset-complexity comparison.

Table 7 reports no-finetuning transfer from ABC to the gauge and connector, using this setting to test how topology-guided protection behaves under scan-domain shifts.

Table 7: Cross-domain Performance Comparison of Sampling Methods

Method	Type	ABC→Rail CD	ABC→Battery CD	Rail Improvement	Battery Improvement
Random	No parameters	0.118	0.164	/	/
FPS	No parameters	0.099	0.152	19.2%	7.3%
Curvature	No parameters	0.095	0.149	19.5%	9.1%
S-NET	Learning-oriented	0.091	0.135	22.9%	17.7%
SampleNet	Learning-oriented	0.088	0.142	25.4%	13.4%

STDN	Learning-oriented	0.076	0.133	35.8%	18.9%

Figure 16 shows the ABC-to-gauge comparison, where STDN obtains the lowest CD among the selected methods.

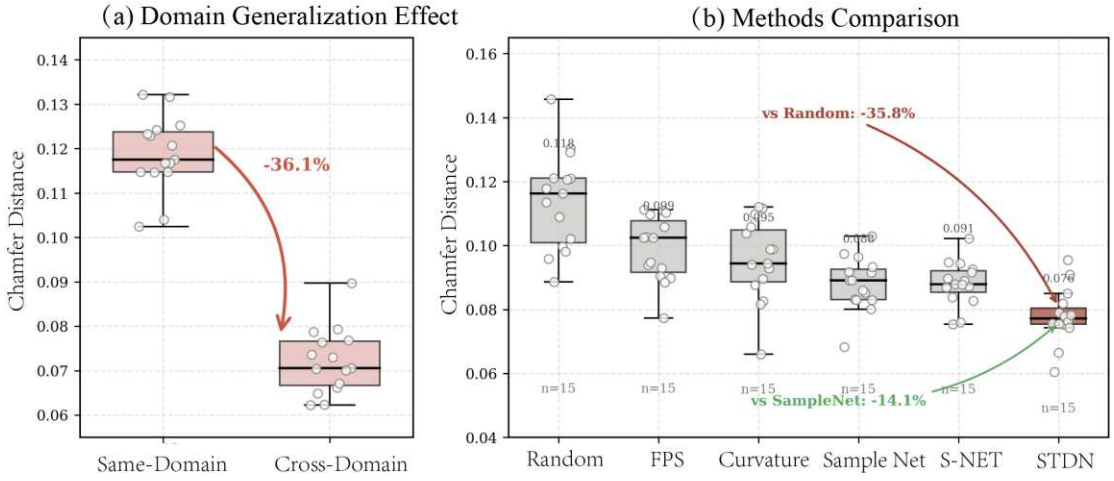


Figure 16: ABC→Standard Gauge cross-domain transfer.

Figure 17 shows the ABC-to-connector test; STDN gives the lowest reported CD among the selected methods in this setting, indicating that the topology-guided protection field remains effective in the more complex connector geometry.[4041]

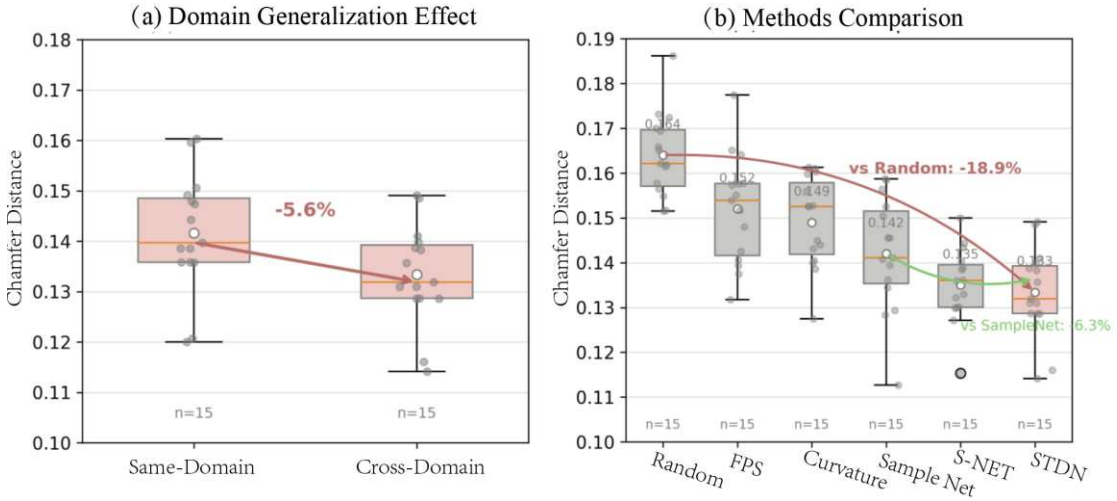


Figure 17: ABC→Battery Connector cross-domain transfer.

Overall, the transfer results indicate that topology-guided sampling can reduce performance degradation across the tested scan domains.

1) Scale decoupling: H-R dynamics use normalized relative geometric features rather than absolute coordinates, supporting transfer across scan scales.
2) These results suggest that ABC's geometric diversity, the topology prior, and source-point selection jointly help the sampler preserve functional structures when

scan scale and component geometry change.

5. Validation of Industrial Geometric Fidelity

Industrial geometric fidelity is evaluated at a 25% sampling rate on the standard-gauge and battery-connector datasets using NFR and ECD.

Table 8: Comparison of Geometric Structure Preservation Degree of Industrial Data Sets

Dataset	Method	Sampled Feature Points	ECD	NFR
Standard specification	Random	3,772	0.0177	25.7%
	FPS	4845	0.0152	53.1%
	Curvature	7289	0.0131	89.3%
	SampleNet	8952	0.0118	83.6%
	S-NET	10086	0.0108	87.2%
	STDN	14955	0.0095	99.7%
Battery pack connector	Random	3759	0.0051	24.7%
	FPS	4720	0.0044	52.1%
	Curvature	6293	0.0035	76.6%
	SampleNet	8288	0.0026	80.4%
	S-NET	9136	0.0021	82.7%
	STDN	14940	0.0008	99.6%

Table 8 reports the highest NFR and lowest ECD for STDN on both industrial datasets, including 99.6% NFR and 0.0008 ECD on the connector scans.

Figure 18 qualitatively supports Table 8: non-STDN methods often fragment boundaries, whereas STDN better preserves closed-loop responses in the tested scans.

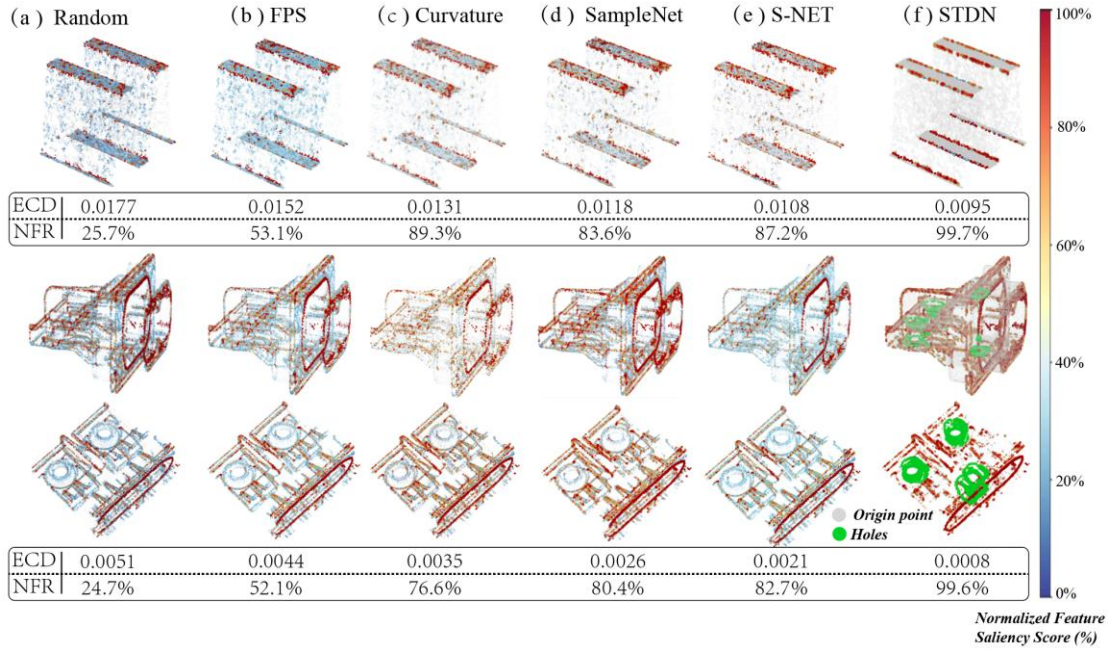


Figure 18: Geometric fidelity on industrial datasets.

The low ECD is consistent with improved boundary connectivity, especially in feature-dense connector regions.

This behavior is consistent with the topological consistency loss, which discourages isolated high-weight nodes and promotes continuous feature support.

5.1 Downstream Assembly Task Validation

The downstream connector case study evaluates whether feature preservation affects pose measurement for circular holes A/B and rectangular slot C.[4243]

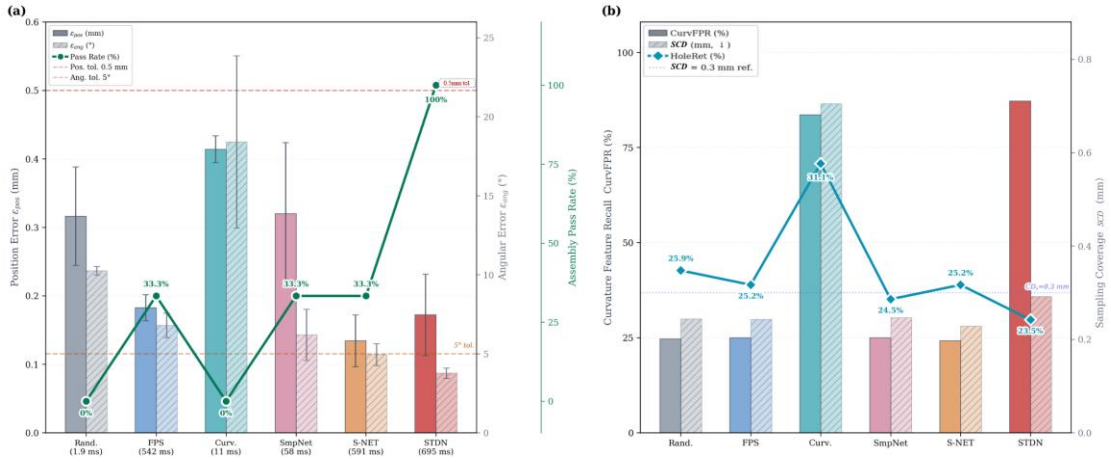


Figure 19: Weighted analysis of connector pose tasks.

Table 9: Comprehensive Evaluation of Downstream Assembly Tasks of Battery Pack Connectors

Method	$\varepsilon_{\mathbf{pos}}$±SEM (mm)	ε_{ang}±SEM (°)	Assembly pass rate	Sampling coverage	CurvFPR	Time-consuming
Random	0.316±0.072	10.25±0.27	(0/3)	0.244	24.7%	2 ms
FPS	0.183±0.019	6.80±0.78	(1/3)	0.243	25.0%	542 ms
Curvature	0.414±0.020	18.41±5.45	(0/3)	0.705	83.6%	11 ms
SampleNet	0.320±0.104	6.20±1.62	(1/3)	0.246	25.0%	58 ms
S-NET	0.134±0.038	4.95±0.69	(1/3)	0.229	24.2%	590 ms
STDN	0.172±0.059	3.77±0.33	(3/3)	0.292	87.2%	695 ms

Table 9 reports an average STDN angular error of 3.77 degrees across the three evaluated connector features, linking boundary-preserving sampling with pose-oriented metrology on the features most affected by down-sampling quality.

Table 9 also shows a tradeoff: S-NET has stronger spatial coverage and translation accuracy, whereas STDN retains more feature-region points and gives lower angular error for the tested features.

Thus, topology-guided sampling reallocates the sampling budget toward pose-sensitive boundaries, while the 695 ms runtime defines a clear target for deployment-oriented acceleration.

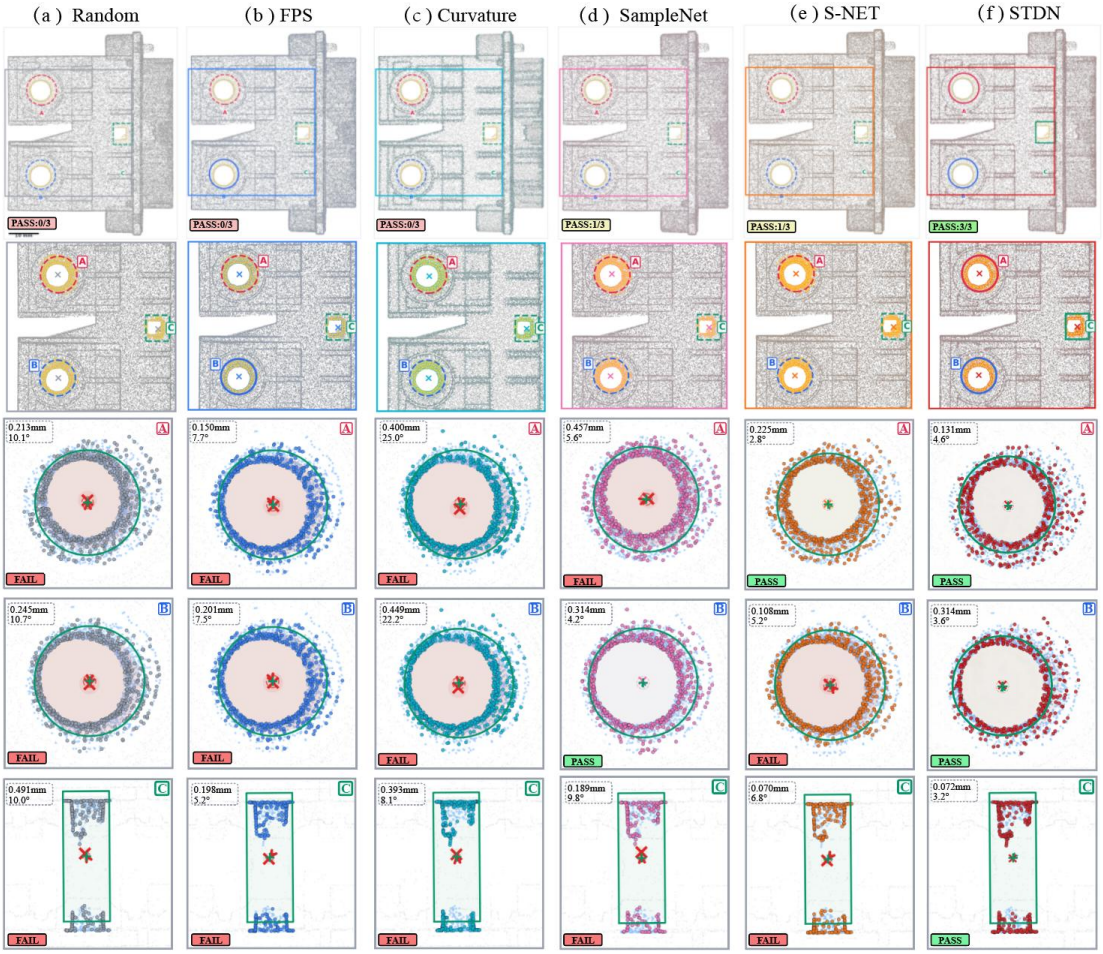


Figure 20: Sampling-driven connector pose quality.

Figure 20 is consistent with Table 9: fragmented boundary sampling corresponds to larger angular errors in this connector case study.

Overall, the connector experiment indicates a task-level benefit under the tested scan conditions and motivates deployment-oriented acceleration in future implementation.

6. Conclusion

This paper addressed industrial point-cloud down-sampling as a feature-continuity knowledge representation problem. The proposed STDN encodes this knowledge through topology-guided source-point sampling, where multi-scale graph propagation, H-R-inspired dynamics, and negative-feedback inhibition protect functional boundaries while suppressing isolated noise responses.

The experimental evidence supports three main findings. First, STDN improves feature-continuity preservation in the tested workpieces, and the ablation results show that dynamic propagation and topological construction both shape the sampled distribution. Second, the ABC-to-industrial tests show that topology-guided protection can retain performance across the evaluated scan-domain shift. Third, the standard-gauge and battery-connector experiments connect sampling quality to industrial consequences, including 99.6% normalized feature recall, 0.0008 edge connectivity dispersion, and an average angular error of 3.77 degrees across the three evaluated connector features.

The central insight is that metrology-oriented sampling should preserve the continuity of functional source-point structures, not only global spatial coverage or local curvature magnitude. STDN implements this insight by turning topology into a protection field on acquired points, making feature continuity an explicit engineering-informatics representation in the reduction process.

Future work will extend this representation across broader public and industrial benchmarks, integrate newer learning-based samplers under unified settings, and couple the sampling objective more directly with inspection and assembly optimization. These directions continue the same principle developed in this paper: point-cloud reduction should preserve the functional geometry that engineering decisions actually use.

Statements and Declarations

Funding

This work was supported by the Jiangsu Provincial Key Research and Development Program (Grant BE2021012-3) and the State Key Laboratory of Mechanical Transmission for Advanced Equipment, Chongqing University (Grant SKLMT-MSKFKT-202325).

Competing Interests

The authors declare that they have no relevant financial or non-financial interests to disclose.

Author Contributions

Zhangchenlong Huang: Methodology, data curation, software, validation, and writing - original draft. Haiying Wen: Software, validation, supervision, and funding acquisition. Zhijie Xia: Methodology and writing - review and editing. Fang Jia: Software. Yilin Tao: Conceptualization and writing - review and editing. Yibo Zhang: Data curation and writing - review and editing. Zhisheng Zhang: Conceptualization, supervision, funding

acquisition, and writing - review and editing. All authors read and approved the final manuscript.

Reference

[1] Rusu R B, Cousins S. 3d is here: Point cloud library (pcl)[C]//2011 IEEE international conference on robotics and automation. IEEE, 2011: 1-4.

[2] Pauly M, Gross M, Kobbelt L P. Efficient simplification of point-sampled surfaces[C]//IEEE Visualization, 2002. VIS 2002. IEEE, 2002: 163-170.

[3] Alexa M, Behr J, Cohen-Or D, et al. Computing and rendering point set surfaces[J]. IEEE Transactions on visualization and computer graphics, 2003, 9(1): 3-15.

[4] Xu X, Li K, Ma Y, et al. Feature-preserving simplification framework for 3D point cloud[J]. Scientific reports, 2022, 12(1): 9450.

[5] Chen S, Tian D, Feng C, Vetro A, Kovacevic J. Fast resampling of three-dimensional point clouds via graphs[J]. IEEE Transactions on Signal Processing, 2018, 66(3): 666-681. doi:10.1109/TSP.2017.2771730.

[6] Qi J, Hu W, Guo Z. Feature Preserving and Uniformity-Controllable Point Cloud Simplification on Graph[C]//2019 IEEE International Conference on Multimedia and Expo (ICME). IEEE, 2019: 284-289. doi:10.1109/ICME.2019.00057.

[7] Lang I, Manor A, Avidan S. Samplenet: Differentiable point cloud sampling[C]//Proceedings of the IEEE/CVF conference on computer vision and pattern recognition. 2020: 7578-7588.

[8] Potamias R A, Bouritsas G, Zafeiriou S. Revisiting point cloud simplification: A learnable feature preserving approach[C]//European conference on computer vision. Cham: Springer Nature Switzerland, 2022: 586-603.

[9] Dovrat O, Lang I, Avidan S. Learning to Sample[C]//2019 IEEE/CVF Conference on Computer Vision and Pattern Recognition (CVPR). IEEE, 2019: 2755-2764. doi:10.1109/CVPR.2019.00287.

[10] Yang J, Zhang Q, Ni B, Li L, Liu J, Zhou M, Tian Q. Modeling Point Clouds With Self-Attention and Gumbel Subset Sampling[C]//2019 IEEE/CVF Conference on Computer Vision and Pattern Recognition (CVPR). IEEE, 2019: 3318-3327. doi:10.1109/CVPR.2019.00344.

[11] C. Qin, H. You, L. Wang, et al., "PointDAN: A Multi-Scale 3D Domain Adaption Network for Point Cloud Representation," in Proc. NeurIPS, 2019.

[12] L. Zou, H. Tang, K. Chen, et al., "Geometry-Aware Self-Training for Unsupervised

Domain Adaptation on Object Point Clouds," in Proc. ICCV, 2021.

[13] J. Wei, G. Gu, and J. Sun, "Learning to Generalize across Domains on Single Test Samples," in Proc. ECCV, 2022.

[14] Eldar Y, Lindenbaum M, Porat M, et al. The farthest point strategy for progressive image sampling[J]. IEEE transactions on image processing, 1997, 6(9): 1305-1315.

[15] Qi C R, Yi L, Su H, et al. Pointnet++: Deep hierarchical feature learning on point sets in a metric space[J]. Advances in neural information processing systems, 2017, 30.

[16] Qian Y, Hou J, Zhang Q, et al. Mops-net: A matrix optimization-driven network fortask-oriented 3d point cloud downsampling[J]. arXiv preprint arXiv:2005.00383, 2020.

[17] Potamias R A, Bouritsas G, Zafeiriou S. Revisiting point cloud simplification: A learnable feature preserving approach[C]//European conference on computer vision. Cham: Springer Nature Switzerland, 2022: 586-603.

[18] Xu X, Li K, Ma Y, et al. Feature-preserving simplification framework for 3D point cloud[J]. Scientific reports, 2022, 12(1): 9450.

[19] Pathak S, Baldwin-McDonald T, Sels S, et al. GP-PCS: One-shot Feature-Preserving Point Cloud Simplification with Gaussian Processes on Riemannian Manifolds[C]//International Conference on Pattern Recognition. Springer, Cham, 2025: 436-452.

[20] Wu N, Liu K, Cheng R, et al. Theia: Gaze-driven and perception-aware volumetric content delivery for mixed reality headsets[C]//Proceedings of the 22nd Annual International Conference on Mobile Systems, Applications and Services. 2024: 70-84.

[21] Lang I, Manor A, Avidan S. Samplenet: Differentiable point cloud sampling[C]//Proceedings of the IEEE/CVF conference on computer vision and pattern recognition. 2020: 7578-7588.

[22] Qian Y, Hou J, Zhang Q, et al. Mops-net: A matrix optimization-driven network fortask-oriented 3d point cloud downsampling[J]. arXiv preprint arXiv:2005.00383, 2020.

[23] Potamias R A, Bouritsas G, Zafeiriou S. Revisiting point cloud simplification: A learnable feature preserving approach[C]//European conference on computer vision. Cham: Springer Nature Switzerland, 2022: 586-603.

[24] Ballerini M, Cabibbo N, Candelier R, et al. Interaction ruling animal collective behavior depends on topological rather than metric distance: Evidence from a field study[J]. Proceedings of the national academy of sciences, 2008, 105(4): 1232-1237.

[25] Kastberger G, Schmelzer E, Kranner I. Social waves in giant honeybees repel hornets[J]. PLoS One, 2008, 3(9): e3141.

[26] Kastberger G, Hoetzl T, Maurer M, et al. Speeding up social waves. Propagation mechanisms of shimmering in giant honeybees[J]. PloS one, 2014, 9(1): e86315.

[27] Sumpter D J T. The principles of collective animal behaviour[J]. Philosophical transactions of the royal society B: Biological Sciences, 2006, 361(1465): 5-22.

[28] Patel N, Huijberts H, Althoefer K, et al. Mathematical Tri-State Model for Bee Shimmering Propagation Dynamics[J]. arXiv preprint arXiv:2401.14145, 2024.

[29] Huang Z, Yu Y, Xu J, et al. Pf-net: Point fractal network for 3d point cloud completion[C]//Proceedings of the IEEE/CVF conference on computer vision and pattern recognition. 2020: 7662-7670.

[30] Landrieu L, Simonovsky M. Large-scale point cloud semantic segmentation with superpoint graphs[C]//Proceedings of the IEEE conference on computer vision and pattern recognition. 2018: 4558-4567.

[31] Lin S, Xiao D, Shi Z, et al. Surface reconstruction from point clouds without normals by parametrizing the gauss formula[J]. ACM Transactions on Graphics, 2022, 42(2): 1-19.

[32] Wang Y, Sun Y, Liu Z, et al. Dynamic graph cnn for learning on point clouds[J]. ACM Transactions on Graphics (tog), 2019, 38(5): 1-12.

[33] Qi C R, Yi L, Su H, et al. Pointnet++: Deep hierarchical feature learning on point sets in a metric space[J]. Advances in neural information processing systems, 2017, 30.

[34] Hindmarsh, J. L., & Rose, R. M. (1984). A model of neuronal bursting using three coupled first order differential equations. *Proceedings of the Royal society of London. Series B. Biological sciences*, 221(1222), 87-102.

[35] Veličković P, Cucurull G, Casanova A, et al. Graph attention networks[J]. arXiv preprint arXiv:1710.10903, 2017.

[36] Chamberlain B, Rowbottom J, Gorinova M I, et al. Grand: Graph neural diffusion[C]//International conference on machine learning. PMLR, 2021: 1407-1418.

[37] Fan H, Su H, Guibas L J. A point set generation network for 3d object reconstruction from a single image[C]//Proceedings of the IEEE conference on computer vision and pattern recognition. 2017: 605-613.

[38] Shuman D I, Narang S K, Frossard P, et al. The emerging field of signal processing on graphs: Extending high-dimensional data analysis to networks and other irregular domains[J]. IEEE signal processing magazine, 2013, 30(3): 83-98.

[39] Yu L, Li X, Fu C W, et al. Pu-net: Point cloud upsampling network[C]//Proceedings of the IEEE conference on computer vision and pattern recognition. 2018: 2790-2799.

[40] Yang H, Zhou Q, Sun H, et al. Pointdgmamba: Domain generalization of point cloud

classification via generalized state space model[C]//Proceedings of the AAAI Conference on Artificial Intelligence. 2025, 39(9): 9193-9201.

[41] Xiao Z, Zhen X, Shao L, et al. Learning to generalize across domains on single test samples[J]. arXiv preprint arXiv:2202.08045, 2022.

[42] T. Hodaň, F. Michel, E. Brachmann, et al., "BOP: Benchmark for 6D Object Pose Estimation," in Proc. European Conference on Computer Vision (ECCV), 2018, pp. 19–34.

[43] J. Tremblay, T. To, B. Sundaralingam, et al., "Deep Object Pose Estimation for Semantic Robotic Grasping of Household Objects," in Proc. Conference on Robot Learning (CoRL), 2018.

Supplementary Files

This is a list of supplementary files associated with this preprint. Click to download.

- HighlightsIJAMT.docx